Research Article Vol. 7, No. 7 / July 2020 / Optica 813

optica

On-demand indistinguishable single photons from an efficient and pure source based on a Rydberg ensemble

D. P. Ornelas-Huerta,[1] A. N. Craddock,[1] E. A. Goldschmidt,[2,3] A. J. Hachtel,[1] Y. Wang,[1] P. Bienias,[1,4] A. V. Gorshkov,[1,4] S. L. Rolston,[1] and J. V. Porto[1,*]

[1]Joint Quantum Institute, NIST/University of Maryland, College Park, Maryland 20742, USA
[2]Department of Physics, University of Illinois at Urbana-Champaign, 1110 W. Green Street, Urbana, Illinois 61801, USA
[3]U.S. Army Research Laboratory, 2800 Powder Mill Road, Adelphi, Maryland 20783, USA
[4]Joint Center for Quantum Information and Computer Science, NIST/University of Maryland, College Park, Maryland 20742, USA
*Corresponding author: porto@umd.edu

Received 5 March 2020; revised 1 May 2020; accepted 9 June 2020 (Doc. ID 391485); published 15 July 2020

Single photons coupled to atomic systems have shown to be a promising platform for developing quantum technologies. Yet a bright on-demand, highly pure, and highly indistinguishable single-photon source compatible with atomic platforms is lacking. In this work, we demonstrate such a source based on a strongly interacting Rydberg system. The large optical nonlinearities in a blockaded Rydberg ensemble convert coherent light into a single collective excitation that can be coherently retrieved as a quantum field. We simultaneously observe a fully single-mode (spectral, temporal, spatial, and polarization) efficiency up to 0.098(2), a detector-background-subtracted $g^{(2)} = 5.0(1.6) \times 10^{-4}$, and indistinguishability of 0.980(7), at an average photon production rate of $1.18(2) \times 10^4\ s^{-1}$. All of these make this system promising for scalable quantum information applications. Furthermore, we investigate the effects of contaminant Rydberg excitations on the source efficiency and observed single-mode efficiencies up to 0.18(2) for lower photon rates. Finally, recognizing that many quantum information protocols require a single photon in a fully single mode, we introduce metrics that take into account all degrees of freedom to benchmark the performance of on-demand sources.

https://doi.org/10.1364/OPTICA.391485

1. INTRODUCTION

Engineering single-photon sources with high efficiency, purity, and indistinguishability is a longstanding goal for applications such as linear optical quantum computation [1], boson sampling [2], quantum networks [3], and quantum metrology [4]. Atomic systems have shown significant progress towards quantum light–matter interfaces, including efficient quantum memories [5], quantum networks [6], high-fidelity light–matter entanglement [7], atomic gates [8], and quantum simulators [9]. Atomic platforms require spectrally matched single photons that can coherently couple with atomic processors, provided with high-efficiency generation, purity, and indistinguishability.

Strongly interacting Rydberg atoms provide a particularly promising system. They have proven to be versatile for engineering strong interactions between photons, exhibiting nonlinearities at the single-photon level [10–13]. Recent experiments using Rydberg interactions have demonstrated on-demand single-photon generation [14,15], as well as photon transistors [16–18], photonic and atomic phase gates [19–24], high-visibility quantum interference in hybrid systems [25], and quantum simulators [26–29].

We describe here an efficient single-photon source based on collective excitation and de-excitation of a cold, trapped ensemble of atoms through a highly excited Rydberg state [14,15,30]. During two-photon excitation from the ground to the Rydberg state via an intermediate state [see Fig. 1(a)], long-range van der Waals interactions suppress multiple Rydberg excitations within a blockade radius, r_b [31]. The resulting single, collective atomic excitation is coherently shared among N atoms as a spin wave [30]. Due to the collective nature of the excitation, if the initial phase coherence of the spin wave is maintained, the subsequent coupling of the Rydberg state to the intermediate state can efficiently map the excitation onto a single photon in a well-defined mode [32]. Our system produces single photons with repetition rates up to 400 kHz, a generation probability up to 0.40(4), $g^{(2)} = 5.0(1.6) \times 10^{-4}$, and indistinguishability of 0.980(7). We model the write and retrieval process, including the measured spin-wave dephasing rate. We identify long-lived contaminant Rydberg states [33] as a limiting factor on the source efficiency for increasing production rates.

Given the requirements for most quantum information applications, the single-mode efficiency, rate, and quality of

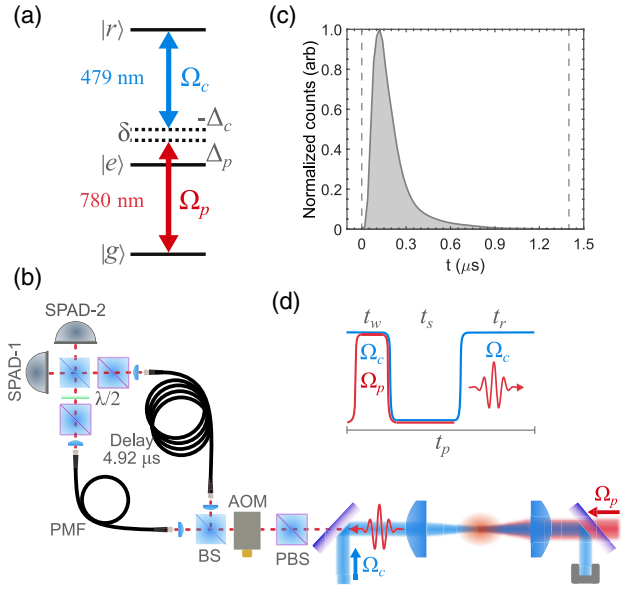

Fig. 1. (a) Relevant atomic levels and setup for single-photon generation. During the spin-wave writing stage, we set the single-photon detuning $\Delta_p/(2\pi) \approx 50$ MHz and the two-photon detuning $\delta = \Delta_p + \Delta_c$ to Raman resonance, $\delta/(2\pi) \approx -2$ MHz. For retrieval, $\Delta_c/(2\pi) \approx 7$ MHz. (b) Experimental setup schematic. There is a polarization beamsplitter (PBS) to project the photons into a single-polarization mode, followed by an acousto-optic modulator (AOM) that shutters the incoming photons during the write pulse. All of the light is directed to the polarization-maintaining fiber (PMF) to realize a purity measurement. For the indistinguishability characterization, we split the light such that the rate is roughly the same at both ports of the second beamsplitter (BS). By rotating the half-wave plate ($\lambda/2$), we can control the relative polarization of the photons coming from the PMF port and the long-delay port. After each port of the final 50:50 BS, the photons are coupled to a single-mode fiber (not shown) connected to a SPAD. (c) Photon temporal envelope. Gray dashed lines indicate the gate window containing more than 99.9% of the pulse. (d) Timing sequence for the generation of successive single photons, the writing π pulse lasts for $t_w \approx 370$ ns. We use a minimum storage time $t_s \approx 350$ ns to maximize the retrieval and vary t_r to change the repetition rate $R = 1/t_p$.

single-photon sources are of key importance since successful scaling of these systems involves the detection of multiple identical photons. Thus, we introduce metrics to describe the probability, rate, and fidelity of producing a single photon in a fully single mode (spectral, temporal, spatial, and polarization), which includes contributions from the commonly used metrics: fibered efficiency, purity, indistinguishability, and repetition rate [34].

2. EXPERIMENTAL APPARATUS AND PROCEDURE

We start the experiment with a magneto-optical trap of ^{87}Rb atoms and further laser cool the atoms with a Λ-gray molasses down to $\approx$10 μK. We load the atoms into a 1003 nm wavelength optical dipole trap. To write the spin wave, we couple the ground state, $|g\rangle = |5S_{1/2}, F = 2, m_F = 2\rangle$ to the Rydberg state $|r\rangle = |139S_{1/2}, m_J = 1/2\rangle$ via the intermediate state $|e\rangle = |5P_{3/2}, F = 3, m_F = 3\rangle$ with an intermediate detuning $\Delta_p/(2\pi) \approx 50$ MHz, as shown in Figure 1(a). The probe beam coupling $|g\rangle$ to $|e\rangle$ is focused into the atom cloud with a waist of $\approx$3.3 μm, with a Rabi frequency $\Omega_p/(2\pi) \approx 1$ MHz. The counter-propagating control beam coupling $|e\rangle$ to $|r\rangle$ has a larger $\approx$19 μm waist and peak Rabi frequency $\Omega_c/(2\pi) \approx 7$ MHz.

The van der Waals coefficient of the Rydberg state $139S_{1/2}$ is $C_6/(2\pi) \approx -2.5 \times 10^6$ GHz μm^6 [35], which results in a blockade radius $r_b \approx 60$ μm during the spin-wave writing. Since r_b is larger than the probe beam waist and the atomic cloud extension in the propagation direction, $\sigma_z \approx 27$ μm, the excitation volume is blockaded, suppressing the storage of more than a single spin-wave excitation in the medium. This is in contrast to other Rydberg systems, where pair-spin-wave dephasing purifies a single-photon excitation [14,15,36]. Furthermore, the effective two-photon Rabi frequency, $\Omega_{2ph} = \frac{\Omega_p \Omega_c}{2\Delta_p}$, is enhanced by a factor of $\sqrt{N} \approx 20$ from the N atoms participating in the collective excitation [30,37].

After a spin-wave storage time $t_s > 350$ ns [see Fig. 1(d)], we turn back on the control field with a detuning $\Delta_c \approx 2\pi \times 7$ MHz that maximizes the retrieval efficiency of the spin wave into a single photon. We can vary the repetition rate of the write–retrieval sequence up to 400 kHz, with interrogation times up to 600 ms (0.6 duty cycle) before we need to reload the optical dipole trap. The generated photons are detected by two single-photon avalanche detectors (SPAD) with a quantum efficiency of $\approx$70% and dark counts (plus background ambient light) of $\approx$90 s^{-1}. The arrival of every event is recorded with an externally triggered time-tagging device, which allows defining of gating windows around the photon pulses and construction of correlation functions off-line after data collection.

3. SINGLE-PHOTON SOURCE PURITY AND INDISTINGUISHABILITY

We use Hanbury Brown–Twiss and Hong–Ou–Mandel interferometers (HOMs) to characterize the purity and indistinguishability of our single photons [see Fig. 1(b)]. The purity of our single-photon source is defined as $1 - g^{(2)}(0)$, where $g^{(2)}(\tau)$ is the second-order autocorrelation function. We apply a 1.4−μs-long gate window starting just before the photon rising edge, as indicated in Fig. 1(c) (for more details on this procedure, see Supplement 1). Coincidences at zero time delay are substantially suppressed, as shown in Fig. 2(a), with strong antibunching $g^{(2)}_{\text{raw}}(0) = 0.0145(2)$, integrating the area around $\tau = 0$ and without background subtraction. The background coincidence rate is dominated by coincidences involving photon events with background counts unrelated to the single-photon generation, coming from detector dark counts and room light leakage. The independently measured background rate, photon shape, and photon rate are constant throughout each experimental run, from which we determine that the accidental coincidences contribute to $g^{(2)}_{\text{back}}(0) = 0.0140$. The gray curve in Fig. 2(b) shows the background coincidence profile within the gate window (see Supplement 1 for details). After background subtraction, our single-photon source has $g^{(2)} = 5.0(1.6) \times 10^{-4}$.

We use a HOM to measure the photon indistinguishability. We implement a fiber-based 4.92 μs delay in one arm to temporally overlap adjacently produced photons. Additionally, there is a polarizing beamsplitter (PBS) at the output of each fiber to account for any polarization rotation due to the fibers. At the exit of the short arm, there is a half-wave plate (HWP) to rotate the polarization and control the degree of distinguishability of the photons. Figure 3(a) shows the normalized coincidences for orthogonal and

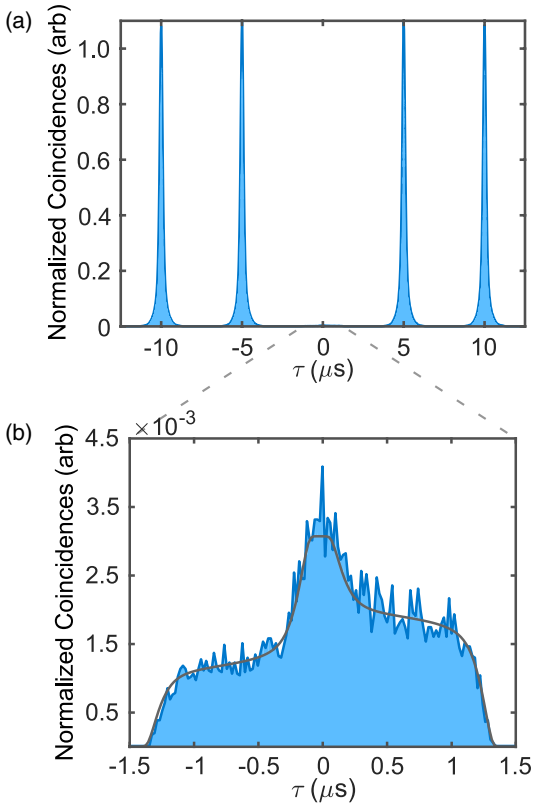

Fig. 2. Measured coincidences for purity and characterization. (a) Normalized coincidences for $g^{(2)}(\tau)$ with 5 μs cycle. (b) Normalized coincidences for $g^{(2)}(\tau)$ around $\tau = 0$, gray line represents the background coincidences with 20 ns bins. The shape of this profile arises from the convolution of the photon pulse shape with a constant background within the gate window, and the pedestal asymmetry is because the background rate is not the same for each channel. All $\sim 2.4 \times 10^9$ pulse cycles for the data shown were taken with 60% duty cycle.

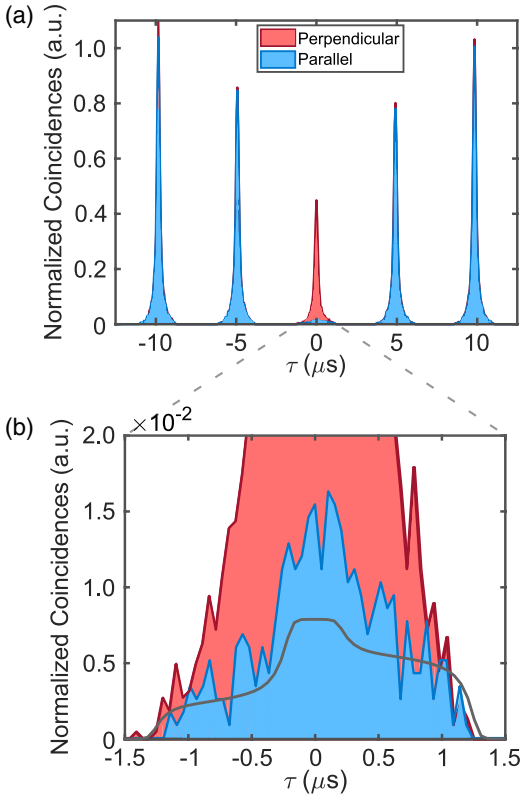

Fig. 3. Measured coincidences for indistinguishability characterization. (a) Normalized coincidences for HOM characterization with 4.92 μs cycle. Indistinguishable polarization states are represented in blue, and distinguishable polarization states are in red. (b) Normalized coincidences for HOM around $\tau = 0$, the gray line represents the background coincidences with 52 ns bins. All $\sim 3 \times 10^8$ pulse cycles for the data shown were taken with 60% duty cycle.

parallel polarizations. Integrating the number of coincidences in a window around $\tau = 0$ for the two cases, we measure a raw HOM interference visibility $\mathcal{V}_{\text{raw}} = 1 - C_{\parallel}/C_{\perp} = 0.892(6)$. Accounting for the accidental coincidences with background events and the slight differences in the transmission and reflection coefficients of our combining beamsplitter gives a mode overlap of 0.980(7) (see Supplement 1).

4. SOURCE EFFICIENCY

We measure a peak fibered efficiency of 0.18(2) after polarization filtering and averaged for a 20% duty cycle. Accounting for optical losses and assuming that the single photon has the same spatial mode as the 780 nm write beam, we estimate a generation probability of 0.40(4) immediately after the atomic ensemble. The average fibered and generation efficiencies reduce to 0.14(1) and 0.31(2), respectively, for a 60% duty cycle.

We calculate $P_{\text{th}} = \eta_w \eta_s \eta_r$ as a product of the writing, η_w, storage, η_s, and retrieval, η_r, efficiencies to estimate the theoretical probability of generating a photon. Referring the reader to Supplement 1 for the details of the theoretical analysis, we summarize it here only briefly. We simulate the writing of the spin wave using a Lindblad master equation to estimate the writing efficiency and storage efficiency. We calculate the retrieval efficiency using the optical Maxwell–Bloch equations with the formalism in Ref. [38]. Using independently measured experimental values as input parameters, we obtain a theoretical prediction of $P_{\text{th}} \approx 0.42(3)$. This value is consistent with the measured generation probability for the longest pulsing periods, t_p.

We observed that the average photon production efficiency decreased at higher repetition rates, as shown in Fig. 4(a). Here, the photon probability is determined immediately after the atom cloud by accounting for independently measured optical losses. The initial pulse in a pulse series had higher efficiency; however, the efficiency of subsequent pulses decreased exponentially to the steady-state value on a ≈60 μs time scale [see Fig. 4(b)].

These observations are consistent with the creation of contaminant atoms in other long-lived Rydberg states that are not removed by the retrieval field. These states interact strongly with the target Rydberg state, affecting subsequent writing events. Similar contaminant states have been observed in previous experiments [33,39,40] and have been analyzed extensively [41–45]. Once a contaminant is in the medium, it disables the writing of a spin wave for the later pulses. Since contaminants have a finite lifetime in the medium, the photon generation probability decreases for shorter pulse periods.

We use a simple model to capture the effect of contaminants on photon production (see Supplement 1 for details). We assume that for any given pulse, there is a probability P_c of creating a contaminant. If the contaminant state has a lifetime τ_c, then the probability P_n of having a contaminant in the nth pulse of a pulse series with period t_p is

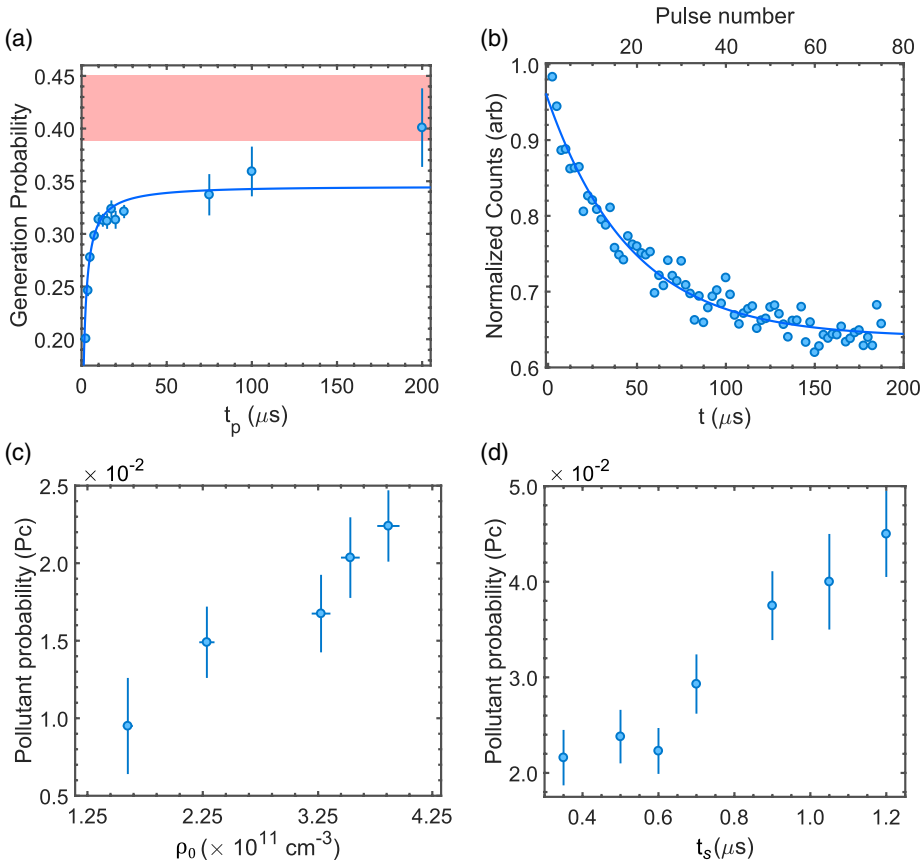

Fig. 4. Effect of contaminants on single-photon generation. (a) Photon generation probability as a function of pulse period t_p. Dark blue line is fitted using Eq. (1) in the steady state for $n \to \infty$ using the values for P_c and τ_c in the main text, and we obtain $P_{\max} = 0.35(2)$. Red band shows the generation probability predicted by the theoretical model. (b) Normalized summed counts per pulse for a pulse train with 2.5 μs pulse period. Dark-blue line is fitted with Eq. (1). (c) P_c versus peak atomic density ρ_0 with a fixed storage $t_s = 350$ ns. (d) P_c versus time t_s with a density of $\approx 4 \times 10^{11}$ cm^{-3}.

$$P_n = P_c \frac{1 - (e^{-t_p/\tau_c} - P_c)^n}{1 - e^{-t_p/\tau_c} + P_c}. \quad (1)$$

For $\tau_c \gg t_p$, the average contaminant probability as $n \to \infty$ can be significant, even if P_c is small. The probability $P_g(n)$ of successfully generating a single photon on the nth pulse in the presence of a contaminant is decreased according to $P_g(n) = P_{\max}(1 - P_n)$, where $P_{\max}$ is the probability of photon generation in the absence of contaminants. The steady state efficiency is given by $P_g(n \to \infty)$. Fitting this equation to pulse sequence data, as shown in Fig. 4(b), we determine $P_c = 1.9(3) \times 10^{-2}$, and $\tau_c = 65(8)$ μs, which is in good agreement with the data in Fig. 4(a).

We find that P_c increases linearly with atomic density ρ [see Fig. 4(c)], which suggests that the source of contaminants is ground-Rydberg interactions. For high principal quantum number n, collisionally produced contaminants were identified in Ref. [42] to be Rydberg states with principal quantum number $n - 4$ and quantum angular momentum $l > 2$. Furthermore, we find that P_c increases with storage time t_s at a rate of $\approx 3 \times 10^{-2}$ μs^{-1}, which gives a contaminant generation time scale of ≈33 μs for a density of $\approx 4 \times 10^{11}$ cm^{-3}. Contaminants are not a fundamental limitation since strong electric field pulses between writing pulses could be used to remove them.

For interrogation times longer than 100 ms, atom loss due to effects such as heating and atom depolarization from rescattering become more significant. For short t_p, where this problem is most prominent, the average probability of generating a photon during 600 ms is ≈75% of the generation probability during the first 100 ms. However, these effects can be mitigated by detuning farther from the intermediate state.

We also note that there was no statistical difference in $g^{(2)}(0)$ as a function of the pulse cycle t_p (to the level of $g^{(2)} \sim 10^{-3}$ for a smaller set of measurements), supporting our hypothesis that contaminants only prevent the spin-wave writing but do not affect the purity. Under the same argument, the indistinguishability should not change with repetition rate, but we were not able to measure it for different delay times.

5. FULLY SINGLE-MODE EFFICIENCY, RATE, AND FIDELITY

There are many metrics used to quantify the various properties of single-photon sources. Optical quantum information schemes are susceptible to errors if they are not implemented with highly pure and indistinguishable single photons. In addition, scaling up quantum information protocols needs high-generation efficiency, since any inefficiency will lead to an exponential decrease of the success probability with system size. Finally, the rate of single-photon production provides a limitation on the practicality of any protocol.

To that end, we define three metrics that quantify these properties: $\mathcal{F}$, the single-photon fidelity, which is the fraction of emission that consists of a single photon in a single spectral, temporal, polarization, and spatial mode; P_1^{sm}, the probability of generating a single photon in the desired mode; and $\mathcal{R}$, the fully single-mode rate, which is the rate of photon production in the desired mode.

Assuming that the probability of multi-photon events greater than two is negligible, the only outcomes from a source are: single photons in the desired mode with probability P_1^{sm}, single photons in an undesirable mode with probability $P_{1'}$, two photons in any mode with probability P_2, and null events with probability P_0. Experimentally, the following quantities are measured: the detector-corrected fibered efficiency P; the HOM visibility, $\mathcal{V}$; and the second-order autocorrelation function, $g^{(2)}$. These are given by

$$P = \frac{1-P_0}{\eta_{\mathrm{det}}} \approx P_1^{\mathrm{sm}} + P_{1'} + (2-\eta_{\mathrm{det}})P_2, \tag{2}$$

$$\mathcal{V} = \frac{P_1^{\mathrm{sm}}}{P_1^{\mathrm{sm}} + P_{1'}}, \tag{3}$$

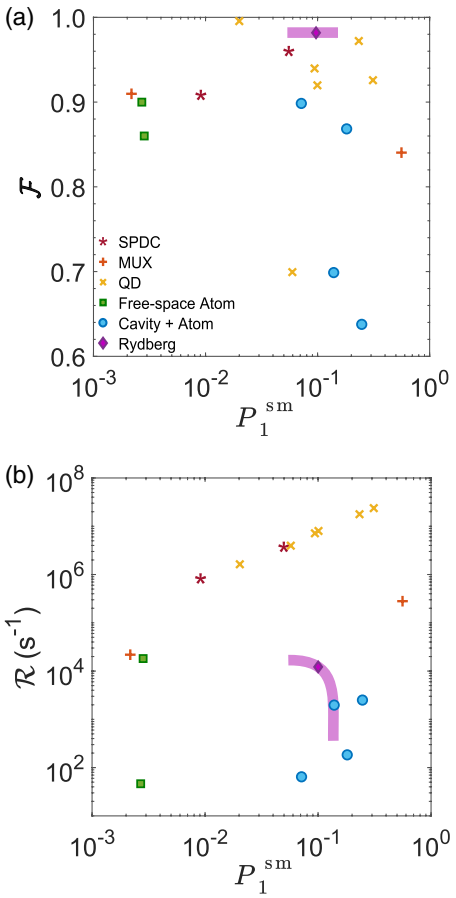

Fig. 5. Performance of a sample from different single-photon sources. Solid-state systems considered are spontaneous parametric down-conversion (SPDC) [46,47], multiplexed-heralded-single-photon source (MUX-HSPS) [48,49], and quantum dots (QD) [50–55]. Atomic systems considered are single atoms in free space [56,57], atoms in cavities [58–61], and this work. The range indicated by the purple shaded area is based on measured efficiencies P, with different pulse periods t_p, assuming $g^{(2)}$ and $\mathcal{V}$ remain unchanged with t_p. (a) Fidelity $\mathcal{F}$ versus fully single-mode single-photon efficiency P_1^{sm}. (b) Single-mode single-photon rate $\mathcal{R}$ versus fully single-mode single-photon efficiency P_1^{sm}. (For details on these sources, see tables in Supplement 1.)

$$g^{(2)} \approx \frac{2P_2}{(P_1^{\mathrm{sm}} + P_{1'})^2}. \tag{4}$$

Here, we have assumed that the measurements are taken with standard non-number-resolving photon-counting detectors with efficiency η_{det}. As seen in Eq. (2), for $\eta_{\mathrm{det}} < 1$, the probability of a detection event from two photons is $(1-(1-\eta_{\mathrm{det}})^2)P_2$ [62]. In Eq. (3), we have assumed that the visibility $\mathcal{V}$ is corrected for multi-photon events (see Supplement 1).

Solving the system of equation for P_1^{sm} to the second order in $g^{(2)}$, we get the fully single-mode efficiency:

$$P_1^{\mathrm{sm}} = P\mathcal{V}\left[1 - \frac{Pg^{(2)}}{2}(2-\eta_{\mathrm{det}})\left(1 - Pg^{(2)}(2-\eta_{\mathrm{det}})\right)\right]. \tag{5}$$

This figure of merit characterizes the efficiency of a fully single-mode single-photon source, including the spectro-temporal coherence measured from the HOM visibility. For many quantum information applications that demand pure indistinguishable single photons, the success probability scales with P_1^{sm} rather than other commonly reported metrics, such as the fibered efficiency P.

We report the source fully single-mode single-photon rate as $\mathcal{R} = R_{\mathrm{eff}}P_1^{\mathrm{sm}}$, where R_{eff} is the clock rate weighted by the experimental duty cycle. Apart from source rate, the fraction of emission in the desirable mode, the fidelity $\mathcal{F}$, also matters for applications:

$$\mathcal{F} = 1 - \frac{P_{1'} + P_2}{P} = \frac{P_1^{\mathrm{sm}}}{P}. \tag{6}$$

In Fig. 5, we show P_1^{sm}, $\mathcal{F}$, and $\mathcal{R}$ for a sample of different single-photon sources. For this comparison, $\eta_{\mathrm{det}} = 1$ was assumed, thus for sources with a non-negligible $g^{(2)}$, P_1^{sm} is an upper bound. Narrow-bandwidth sources naturally compatible with coherent atomic systems are indicated with filled symbols.

6. CONCLUSION

By using the quantum nonlinearities of strongly interacting Rydberg states in a cold atomic ensemble, we demonstrated a single-photon source, operating with a 60% duty cycle, single-mode efficiency of $P_1^{\mathrm{sm}} = 0.098(2)$, a single-mode rate of $\mathcal{R} = 1.18(2) \times 10^4\ \mathrm{s}^{-1}$, and single-mode fidelity of $\mathcal{F} = 0.980(7)$. This fidelity is the highest reported to our knowledge for an atomic-based source. Furthermore, we investigated the limitations of our current setup arising from nearby long-lived contaminant states.

Implementing feasible improvements to the current experiment, we estimate that we can achieve up to $P_1^{\mathrm{sm}} \approx 0.4$, and, moreover, ionizing pulses after each write–retrieval pulse to remove atoms in pollutant states may increase the rate up to $\mathcal{R} \approx 1.2 \times 10^5\ \mathrm{s}^{-1}$ without decreasing the duty cycle or the fidelity (see Supplement 1 for details). The efficiency could be further improved if the ensemble were coupled to a cavity [63]. Given their high efficiency, rate, and fidelity, we have shown that single-photon sources based on Rydberg atomic ensembles provide a promising platform for scalable quantum photonics, for example, boson sampling and quantum networking. Furthermore, they are inherently compatible with narrow-bandwidth atomic platforms that have shown significant progress towards quantum information applications [25].

Funding. United States Army Research Laboratory Center for Distributed Quantum Information; Army Research Laboratory; National Science Foundation Physics Frontier Center (PHY1430094); Air Force Office of Scientific Research; Army Research Office Multidisciplinary University Research Initiative; Department of Energy Advanced Scientific Computing Research Quantum Testbed Pathfinder (DE-SC0019040).

Acknowledgment. All authors acknowledge support from the United States Army Research Lab's Center for Distributed Quantum Information (CDQI) at the University of Maryland and the Army Research Lab. A. C., D. O.-H, A. J. H., S. L. R., J. V. P., Y. W., P. B., and A. V. G. additionally acknowledge support from the National Science Foundation Physics Frontier Center at the Joint Quantum Institute (PHYS-1430094). Y. W., P. B., and A. V. G. additionally acknowledge support from AFOSR, ARO MURI, and DoE ASCR Quantum Testbed Pathfinder program. We are grateful to Mary Lyon for her significant contributions to the design and construction of the apparatus and Patrick Banner for his contributions to data collection. We also want to thank Luis A. Orozco for fruitful discussions (DE-SC0019040).

Disclosures. The authors declare no conflicts of interest.

Please see Supplement 1 for supporting content.

REFERENCES

1. J. Carolan, C. Harrold, C. Sparrow, E. Martín-López, N. J. Russell, J. W. Silverstone, P. J. Shadbolt, N. Matsuda, M. Oguma, M. Itoh, G. D. Marshall, M. G. Thompson, J. C. F. Matthews, T. Hashimoto, J. L. O'Brien, and A. Laing, "Universal linear optics," Science **349**, 711–716 (2015).
2. H. Wang, J. Qin, X. Ding, M.-C. Chen, S. Chen, X. You, Y.-M. He, X. Jiang, L. You, Z. Wang, C. Schneider, J. J. Renema, S. Höfling, C.-Y. Lu, and J.-W. Pan, "Boson sampling with 20 input photons and a 60-mode interferometer in a 1014-dimensional Hilbert space," Phys. Rev. Lett. **123**, 250503 (2019).
3. J. Yin, Y. Cao, Y.-H. Li, S.-K. Liao, L. Zhang, J.-G. Ren, W.-Q. Cai, W.-Y. Liu, B. Li, H. Dai, G.-B. Li, Q.-M. Lu, Y.-H. Gong, Y. Xu, S.-L. Li, F.-Z. Li, Y.-Y. Yin, Z.-Q. Jiang, M. Li, J.-J. Jia, G. Ren, D. He, Y.-L. Zhou, X.-X. Zhang, N. Wang, X. Chang, Z.-C. Zhu, N.-L. Liu, Y.-A. Chen, C.-Y. Lu, R. Shu, C.-Z. Peng, J.-Y. Wang, and J.-W. Pan, "Satellite-based entanglement distribution over 1200 kilometers," Science **356**, 1140–1144 (2017).
4. S. Slussarenko, M. M. Weston, H. M. Chrzanowski, L. K. Shalm, V. B. Verma, S. W. Nam, and G. J. Pryde, "Unconditional violation of the shot-noise limit in photonic quantum metrology," Nat. Photonics **11**, 700–703 (2017).
5. Y. Wang, J. Li, S. Zhang, K. Su, Y. Zhou, K. Liao, S. Du, H. Yan, and S.-L. Zhu, "Efficient quantum memory for single-photon polarization qubits," Nat. Photonics **13**, 346–351 (2019).
6. Y. Yu, F. Ma, X.-Y. Luo, B. Jing, P.-F. Sun, R.-Z. Fang, C.-W. Yang, H. Liu, M.-Y. Zheng, W.-P. Xie, W.-J. Zhang, L.-X. You, Z. Wang, T.-Y. Chen, Q. Zhang, X.-H. Bao, and J.-W. Pan, "Entanglement of two quantum memories via fibres over dozens of kilometres," Nature **578**, 240–245 (2020).
7. M. Bock, P. Eich, S. Kucera, M. Kreis, A. Lenhard, C. Becher, and J. Eschner, "High-fidelity entanglement between a trapped ion and a telecom photon via quantum frequency conversion," Nat. Commun. **9**, 1998 (2018).
8. C. J. Ballance, T. P. Harty, N. M. Linke, M. A. Sepiol, and D. M. Lucas, "High-fidelity quantum logic gates using trapped-ion hyperfine qubits," Phys. Rev. Lett. **117**, 060504 (2016).
9. C. Gross and I. Bloch, "Quantum simulations with ultracold atoms in optical lattices," Science **357**, 995–1001 (2017).
10. T. Peyronel, O. Firstenberg, Q.-Y. Liang, S. Hofferberth, A. V. Gorshkov, T. Pohl, M. D. Lukin, and V. Vuletić, "Quantum nonlinear optics with single photons enabled by strongly interacting atoms," Nature **488**, 57–60 (2012).
11. D. Maxwell, D. J. Szwer, D. Paredes-Barato, H. Busche, J. D. Pritchard, A. Gauguet, K. J. Weatherill, M. P. A. Jones, and C. S. Adams, "Storage and control of optical photons using Rydberg polaritons," Phys. Rev. Lett. **110**, 103001 (2013).
12. L. Li and A. Kuzmich, "Quantum memory with strong and controllable Rydberg-level interactions," Nat. Commun. **7**, 13618 (2016).
13. A. Paris-Mandoki, C. Braun, J. Kumlin, C. Tresp, I. Mirgorodskiy, F. Christaller, H. P. Büchler, and S. Hofferberth, "Free-space quantum electrodynamics with a single Rydberg superatom," Phys. Rev. X **7**, 041010 (2017).
14. Y. O. Dudin and A. Kuzmich, "Strongly interacting Rydberg excitations of a cold atomic gas," Science **336**, 887–889 (2012).
15. F. Ripka, H. Kübler, R. Löw, and T. Pfau, "A room-temperature single-photon source based on strongly interacting Rydberg atoms," Science **362**, 446–449 (2018).
16. H. Gorniaczyk, C. Tresp, J. Schmidt, H. Fedder, and S. Hofferberth, "Single-photon transistor mediated by interstate Rydberg interactions," Phys. Rev. Lett. **113**, 053601 (2014).
17. D. Tiarks, S. Baur, K. Schneider, S. Dürr, and G. Rempe, "Single-photon transistor using a Förster resonance," Phys. Rev. Lett. **113**, 053602 (2014).
18. H. Gorniaczyk, C. Tresp, P. Bienias, A. Paris Mandoki, W. Li, I. Mirgorodskiy, H. Büchler, I. Lesanovsky, and S. Hofferberth, "Enhancement of Rydberg-mediated single-photon nonlinearities by electrically tuned Förster resonances," Nat. Commun. **7**, 12480 (2016).
19. D. Tiarks, S. Schmidt, G. Rempe, and S. Dürr, "Optical π phase shift created with a single-photon pulse," Sci. Adv. **2**, e1600036 (2016).
20. J. D. Thompson, T. L. Nicholson, Q.-Y. Liang, S. H. Cantu, A. V. Venkatramani, S. Choi, I. A. Fedorov, D. Viscor, T. Pohl, M. D. Lukin, and V. Vuletić, "Symmetry-protected collisions between strongly interacting photons," Nature **542**, 206–209 (2017).
21. D. Tiarks, S. Schmidt-Eberle, T. Stolz, G. Rempe, and S. Dürr, "A photon–photon quantum gate based on Rydberg interactions," Nat. Phys. **15**, 124–126 (2019).
22. K. M. Maller, M. T. Lichtman, T. Xia, Y. Sun, M. J. Piotrowicz, A. W. Carr, L. Isenhower, and M. Saffman, "Rydberg-blockade controlled-not gate and entanglement in a two-dimensional array of neutral-atom qubits," Phys. Rev. A **92**, 022336 (2015).
23. Y. Zeng, P. Xu, X. He, Y. Liu, M. Liu, J. Wang, D. J. Papoular, G. V. Shlyapnikov, and M. Zhan, "Entangling two individual atoms of different isotopes via Rydberg blockade," Phys. Rev. Lett. **119**, 160502 (2017).
24. H. Levine, A. Keesling, A. Omran, H. Bernien, S. Schwartz, A. S. Zibrov, M. Endres, M. Greiner, V. Vuletić, and M. D. Lukin, "High-fidelity control and entanglement of Rydberg-atom qubits," Phys. Rev. Lett. **121**, 123603 (2018).
25. A. N. Craddock, J. Hannegan, D. P. Ornelas-Huerta, J. D. Siverns, A. J. Hachtel, E. A. Goldschmidt, J. V. Porto, Q. Quraishi, and S. L. Rolston, "Quantum interference between photons from an atomic ensemble and a remote atomic ion," Phys. Rev. Lett. **123**, 213601 (2019).
26. P. Schauß, M. Cheneau, M. Endres, T. Fukuhara, S. Hild, A. Omran, T. Pohl, C. Gross, S. Kuhr, and I. Bloch, "Observation of spatially ordered structures in a two-dimensional Rydberg gas," Nature **491**, 87–91 (2012).
27. J. Zeiher, J.-Y. Choi, A. Rubio-Abadal, T. Pohl, R. van Bijnen, I. Bloch, and C. Gross, "Coherent many-body spin dynamics in a long-range interacting Ising chain," Phys. Rev. X **7**, 041063 (2017).
28. V. Lienhard, S. de Léséleuc, D. Barredo, T. Lahaye, A. Browaeys, M. Schuler, L.-P. Henry, and A. M. Läuchli, "Observing the space- and time-dependent growth of correlations in dynamically tuned synthetic Ising models with antiferromagnetic interactions," Phys. Rev. X **8**, 021070 (2018).
29. H. Kim, Y. Park, K. Kim, H.-S. Sim, and J. Ahn, "Detailed balance of thermalization dynamics in Rydberg-atom quantum simulators," Phys. Rev. Lett. **120**, 180502 (2018).
30. M. Saffman and T. G. Walker, "Creating single-atom and single-photon sources from entangled atomic ensembles," Phys. Rev. A **66**, 065403 (2002).

31. M. D. Lukin, M. Fleischhauer, R. Cote, L. M. Duan, D. Jaksch, J. I. Cirac, and P. Zoller, "Dipole blockade and quantum information processing in mesoscopic atomic ensembles," Phys. Rev. Lett. **87**, 037901 (2001).
32. N. Sangouard, C. Simon, H. de Riedmatten, and N. Gisin, "Quantum repeaters based on atomic ensembles and linear optics," Rev. Mod. Phys. **83**, 33–80 (2011).
33. E. A. Goldschmidt, T. Boulier, R. C. Brown, S. B. Koller, J. T. Young, A. V. Gorshkov, S. L. Rolston, and J. V. Porto, "Anomalous broadening in driven dissipative Rydberg systems," Phys. Rev. Lett. **116**, 113001 (2016).
34. M. D. Eisaman, J. Fan, A. Migdall, and S. V. Polyakov, "Invited review article: single-photon sources and detectors," Rev. Sci. Instrum. **82**, 071101 (2011).
35. N. Šibalić, J. D. Pritchard, C. S. Adams, and K. J. Weatherill, "Arc: an open-source library for calculating properties of alkali Rydberg atoms," Comput. Phys. Commun. **220**, 319–331 (2017).
36. F. Bariani, P. M. Goldbart, and T. A. B. Kennedy, "Dephasing dynamics of Rydberg atom spin waves," Phys. Rev. A **86**, 041802 (2012).
37. Y. Dudin, L. Li, F. Bariani, and A. Kuzmich, "Observation of coherent many-body Rabi oscillations," Nat. Phys. **8**, 790–794 (2012).
38. A. V. Gorshkov, A. André, M. D. Lukin, and A. S. Sørensen, "Photon storage in Λ-type optically dense atomic media. II. Free-space model," Phys. Rev. A **76**, 033805 (2007).
39. B. J. DeSalvo, J. A. Aman, C. Gaul, T. Pohl, S. Yoshida, J. Burgdörfer, K. R. A. Hazzard, F. B. Dunning, and T. C. Killian, "Rydberg-blockade effects in Autler–Townes spectra of ultracold strontium," Phys. Rev. A **93**, 022709 (2016).
40. D. P. Sadler, E. M. Bridge, D. Boddy, A. D. Bounds, N. C. Keegan, G. Lochead, M. P. A. Jones, and B. Olmos, "Radiation trapping in a dense cold Rydberg gas," Phys. Rev. A **95**, 013839 (2017).
41. J. A. Aman, B. J. DeSalvo, F. B. Dunning, T. C. Killian, S. Yoshida, and J. Burgdörfer, "Trap losses induced by near-resonant Rydberg dressing of cold atomic gases," Phys. Rev. A **93**, 043425 (2016).
42. M. Schlagmüller, T. C. Liebisch, F. Engel, K. S. Kleinbach, F. Böttcher, U. Hermann, K. M. Westphal, A. Gaj, R. Löw, S. Hofferberth, T. Pfau, J. Pérez-Ríos, and C. H. Greene, "Ultracold chemical reactions of a single Rydberg atom in a dense gas," Phys. Rev. X **6**, 031020 (2016).
43. T. Boulier, E. Magnan, C. Bracamontes, J. Maslek, E. A. Goldschmidt, J. T. Young, A. V. Gorshkov, S. L. Rolston, and J. V. Porto, "Spontaneous avalanche dephasing in large Rydberg ensembles," Phys. Rev. A **96**, 053409 (2017).
44. J. T. Young, T. Boulier, E. Magnan, E. A. Goldschmidt, R. M. Wilson, S. L. Rolston, J. V. Porto, and A. V. Gorshkov, "Dissipation-induced dipole blockade and antiblockade in driven Rydberg systems," Phys. Rev. A **97**, 023424 (2018).
45. P. Bienias, J. Douglas, A. Paris-Mandoki, P. Titum, I. Mirgorodskiy, C. Tresp, E. Zeuthen, M. J. Gullans, M. Manzoni, S. Hofferberth, D. Chang, and A. V. Gorshkov, "Photon propagation through dissipative Rydberg media at large input rates," arXiv:1807.07586 (2018).
46. X.-L. Wang, L.-K. Chen, W. Li, H.-L. Huang, C. Liu, C. Chen, Y.-H. Luo, Z.-E. Su, D. Wu, Z.-D. Li, H. Lu, Y. Hu, X. Jiang, C.-Z. Peng, L. Li, N.-L. Liu, Y.-A. Chen, C.-Y. Lu, and J.-W. Pan, "Experimental ten-photon entanglement," Phys. Rev. Lett. **117**, 210502 (2016).
47. H.-S. Zhong, Y. Li, W. Li, L.-C. Peng, Z.-E. Su, Y. Hu, Y.-M. He, X. Ding, W. Zhang, H. Li, L. Zhang, Z. Wang, L. You, X.-L. Wang, X. Jiang, L. Li, Y.-A. Chen, N.-L. Liu, C.-Y. Lu, and J.-W. Pan, "12-photon entanglement and scalable scattershot boson sampling with optimal entangled-photon pairs from parametric down-conversion," Phys. Rev. Lett. **121**, 250505 (2018).
48. C. Xiong, X. Zhang, Z. Liu, M. J. Collins, A. Mahendra, L. G. Helt, M. J. Steel, D.-Y. Choi, C. J. Chae, P. H. W. Leong, and B. J. Eggleton, "Active temporal multiplexing of indistinguishable heralded single photons," Nat. Commun. **7**, 10853 (2016).
49. F. Kaneda and P. G. Kwiat, "High-efficiency single-photon generation via large-scale active time multiplexing," Sci. Adv. **5**, eaaw8586 (2019).
50. N. Somaschi, V. Giesz, L. De Santis, J. C. Loredo, M. P. Almeida, G. Hornecker, S. L. Portalupi, T. Grange, C. Antón, J. Demory, C. Gómez, I. Sagnes, N. D. Lanzillotti-Kimura, A. Lemaítre, A. Auffeves, A. G. White, L. Lanco, and P. Senellart, "Near-optimal single-photon sources in the solid state," Nat. Photonics **10**, 340–345 (2016).
51. J. C. Loredo, N. A. Zakaria, N. Somaschi, C. Anton, L. de Santis, V. Giesz, T. Grange, M. A. Broome, O. Gazzano, G. Coppola, I. Sagnes, A. Lemaitre, A. Auffeves, P. Senellart, M. P. Almeida, and A. G. White, "Scalable performance in solid-state single-photon sources," Optica **3**, 433–440 (2016).
52. H. Wang, Y. He, Y.-H. Li, Z.-E. Su, B. Li, H.-L. Huang, X. Ding, M.-C. Chen, C. Liu, J. Qin, J.-P. Li, Y.-M. He, C. Schneider, M. Kamp, C.-Z. Peng, S. Höfling, C.-Y. Lu, and J.-W. Pan, "High-efficiency multiphoton boson sampling," Nat. Photonics **11**, 361–365 (2017).
53. G. Kiršanskė, H. Thyrrestrup, R. S. Daveau, C. L. Dreeßen, T. Pregnolato, L. Midolo, P. Tighineanu, A. Javadi, S. Stobbe, R. Schott, A. Ludwig, A. D. Wieck, S. I. Park, J. D. Song, A. V. Kuhlmann, I. Söllner, M. C. Löbl, R. J. Warburton, and P. Lodahl, "Indistinguishable and efficient single photons from a quantum dot in a planar nanobeam waveguide," Phys. Rev. B **96**, 165306 (2017).
54. H. Wang, Y.-M. He, T.-H. Chung, H. Hu, Y. Yu, S. Chen, X. Ding, M.-C. Chen, J. Qin, X. Yang, R.-Z. Liu, Z.-C. Duan, J.-P. Li, S. Gerhardt, K. Winkler, J. Jurkat, L.-J. Wang, N. Gregersen, Y.-H. Huo, Q. Dai, S. Yu, S. Höfling, C.-Y. Lu, and J.-W. Pan, "Towards optimal single-photon sources from polarized microcavities," Nat. Photonics **13**, 770–775 (2019).
55. H. Ollivier, I. Maillette de Buy Wenniger, S. Thomas, S. Wein, A. Harouri, G. Coppola, P. Hilaire, C. Millet, A. Lemaitre, I. Sagnes, O. Krebs, L. Lanco, J. Loredo, C. Anton-Solanas, N. Somaschi, and P. Senellart, "Reproducibility of high-performance quantum dot single-photon sources," ACS Photon. **7**, 1050–1059 (2020).
56. P. Maunz, D. Moehring, S. Olmschenk, K. Younge, D. Matsukevich, and C. Monroe, "Quantum interference of photon pairs from two remote trapped atomic ions," Nat. Phys. **3**, 538–541 (2007).
57. W. Rosenfeld, D. Burchardt, R. Garthoff, K. Redeker, N. Ortegel, M. Rau, and H. Weinfurter, "Event-ready bell test using entangled atoms simultaneously closing detection and locality loopholes," Phys. Rev. Lett. **119**, 010402 (2017).
58. J. K. Thompson, J. Simon, H. Loh, and V. Vuletić, "A high-brightness source of narrowband, identical-photon pairs," Science **313**, 74–77 (2006).
59. T. Wilk, S. C. Webster, H. P. Specht, G. Rempe, and A. Kuhn, "Polarization-controlled single photons," Phys. Rev. Lett. **98**, 063601 (2007).
60. P. B. R. Nisbet-Jones, J. Dilley, D. Ljunggren, and A. Kuhn, "Highly efficient source for indistinguishable single photons of controlled shape," New J. Phys. **13**, 103036 (2011).
61. M. Mücke, J. Bochmann, C. Hahn, A. Neuzner, C. Nölleke, A. Reiserer, G. Rempe, and S. Ritter, "Generation of single photons from an atom-cavity system," Phys. Rev. A **87**, 063805 (2013).
62. P. Kok, W. J. Munro, K. Nemoto, T. C. Ralph, J. P. Dowling, and G. J. Milburn, "Linear optical quantum computing with photonic qubits," Rev. Mod. Phys. **79**, 135–174 (2007).
63. L. W. Clark, N. Jia, N. Schine, C. Baum, A. Georgakopoulos, and J. Simon, "Interacting Floquet polaritons," Nature **571**, 532–536 (2019).